Published in final edited form as:
Mol Imaging Biol. 2013 April ; 15(2): . doi:10.1007/s11307-012-0582-y.

Evaluation of [^{18}F]Mefway Biodistribution and Dosimetry Based on Whole-Body PET Imaging of Mice

Cristian C. Constantinescu, **Evgueni Sevrioukov**, **Adriana Garcia**, **Min-Liang Pan**, and **Jogeshwar Mukherjee**
Preclinical Imaging, Department of Radiological Sciences, University of California, Irvine, CA 92697, USA

Abstract

Purpose—[^{18}F]Mefway is a novel radiotracer specific to the serotonin 5-HT$_{1A}$ receptor class. In preparation for using this tracer in humans, we have performed whole-body PET studies in mice to evaluate the biodistribution and dosimetry of [^{18}F]Mefway.

Methods—Six mice (three females and three males) received IV injections of [^{18}F]Mefway and were scanned for 2 h in an Inveon-dedicated PET scanner. Each animal also received a high-resolution CT scan using an Inveon CT. The CT images were used to draw volume of interest on the following organs: the brain, large intestine, stomach, heart, kidneys, liver, lungs, pancreas, bone, spleen, testes, thymus, gallbladder, uterus, and urinary bladder. All organ time-activity curves without decay correction were normalized to the injected activity. The area under the normalized curves was then used to compute the residence times in each organ. Data were analyzed using PMOD and Matlab software. The absorbed doses in mouse organs were computed using the RAdiation Dose Assessment Resource animal models for dose assessment. The residence times in mouse organs were converted to human values using scale factors based on differences between organ and body weights. OLINDA/EXM 1.1 software was used to compute the absorbed human doses in multiple organs for both female and male phantoms.

Results—The highest mouse residence times were found in the liver, urinary bladder, and kidneys. The largest doses in mice were found in the urinary bladder (critical organ), kidney, and liver for both females and males, indicating primary elimination via urinary system. The projected human effective doses were 1.21E–02 mSv/MBq for the adult female model and 1.13E–02 mSv/MBq for the adult male model. The estimated human biodistribution of [^{18}F]Mefway was similar to that of [^{11}C]WAY 100,635, a 5-HT$_{1A}$ tracer for which dosimetry has been evaluated in humans.

Conclusions—The elimination of radiotracer was primarily via the kidney and urinary bladder with the urinary bladder being the critical organ. Whole-body mouse imaging can be used as a preclinical tool to provide initial estimates of the absorbed doses of [^{18}F]Mefway in humans.

Keywords

[^{18}F]Mefway; Dosimetry; Biodistribution; 5-HT$_{1A}$; PET; Preclinical; Whole-body

Correspondence to: Cristian C. Constantinescu; constant@uci.edu.

Conflict of Interest. None

Introduction

Serotonin $5HT_{1A}$ receptors are of interest for imaging and therapeutic applications and have therefore been a target for continued development of effective PET radioligands [1, 2]. Imaging serotonin neurotransmitter system in mood disorders, including depression, sleep disorders, mania, bipolar disorder, anxiety, and others, has been an area of major focus [3, 4]. Relevance of 5-HT_{1A} receptor imaging in epilepsy for surgical planning has been incrementally established [5]. Two areas of potential clinical applications include major depression and epilepsy (reviewed in Parsey [6]). A number of animal model studies have suggested that serotonin 5-HT_{1A} receptors have a role in learning and memory [7, 8].

Several PET radioligands for 5-HT_{1A} receptors have been developed based on the antagonist, WAY-100635. Three derivatives are currently in human studies ([^{11}C]WAY-100635, [^{18}F]FCWAY, and [^{18}F]MPPF). For several reasons, efforts are still underway to improve the biological properties of currently used 5-HT_{1A} agents for human studies [2, 9]. Our goal was to develop a fluorinated radiotracer for 5-HT_{1A} receptors that would be relatively more stable to metabolism, easily synthesized, and would retain high affinity and selectivity for the 5-HT_{1A} receptors. Thus, Mefway was synthesized as an analog of WAY-100635 and labeled with fluorine-18 to provide [^{18}F]Mefway (Fig. 1, [9]).

[^{18}F]Mefway is a highly selective serotonin 5-HT_{1A} receptor radioligand that has been shown to yield high specific/nonspecific ratios in nonhuman primates *in vivo* [9]. Rodent-imaging studies, using [^{18}F]Mefway, have also been reported [10]. [^{18}F]Mefway presents interest because of its high binding sensitivity in regions with low and medium 5-HT_{1A} receptor densities, which has been demonstrated in studies of nonhuman primates [11]. Comparative studies have shown a high signal-to-noise ratio of [^{18}F]Mefway measurements compared to those using a carbon-11-labeled tracer with similar kinetics, [C-11]WAY100635, due to longer half-life of fluorine-18. [^{18}F]Mefway kinetics and quantification have been studied in nonhuman primates using PET [11]. The promising characteristics of [^{18}F] Mefway makes this tracer a good candidate for use in humans.

In this work, we evaluated the *in vivo* biodistribution of [^{18}F]-*trans*-Mefway (heretofore referred as [^{18}F]Mefway) in the mouse organs using whole-body PET and CT imaging. Residence times were computed for several mouse organs, and absorbed doses were then derived using the RAdiation Dose Assessment Resource (RADAR) models for dose assessment developed at Vanderbilt University [12, 13]. The mouse residence times were extrapolated to humans based on simple assumptions on difference between the species. We used OLINDA/EXM 1.1 dosimetry software to derive human organ doses for both adult female and male phantoms based on the projected residence times.

Materials and Methods

Tracer Synthesis

[^{18}F]Mefway was synthesized as reported in Saigal et al. [9]. The radiosynthesis was performed using an automated Chemistry Process Control Unit (CPCU) and fluorine-18 in $H_2{}^{18}O$ from an MC-17 cyclotron, which was passed through a QMA-light Sep-Pak (Waters Corp.), preconditioned with 3 ml of K_2CO_3 (140 mg/ml), and followed by 3 ml of anhydrous acetonitrile. The ^{18}F trapped in the QMA-light Sep-Pak was then eluted with 1 ml Kryptofix 2.2.2/K_2CO_3 (360/75 mg in 1 ml of water and 24 ml of acetonitrile) and transferred to the CPCU reaction vessel. The SYNTH1 program in the CPCU was used for the synthesis. The CH_3OH was removed in vacuum, and the residue was taken for HPLC purification. The product was purified in a reverse-phase HPLC C18 Econosil column (250×10 mm; Alltech Assoc., Inc.) with 60 % acetonitrile, 40 % water containing 0.1 %

triethylamine with a flow rate of 2.5 ml/min. Fluorine-18 radioactivity was counted in a dose calibrator (CRC-15R, Capintec). The specific activity of [^{18}F] Mefway exceeded 74 GBq/μmol at the end of synthesis.

Subjects

This study was conducted under protocols approved by the Institutional Animal Care and Use Committee of University of California, Irvine. Six mice, three females, and three males, weighing 30±2 g, were used for this study. The animals were separated based on gender and housed in cages in a climate-controlled room (24.4 °C), with a 12:12-h light cycle. Subjects had free access to food and water during housing. Subjects were fasted for 24 h prior to PET imaging. In preparation for the scans, the mice were induced into anesthesia with 4 % isoflurane.

PET and CT Scanning

Animals received IV tail injections (9.48±2.88 MBq) of [^{18}F] Mefway outside the Inveon Multimodality (MM) scanner (Siemens Medical Solutions, Knoxville, TN) and immediately were placed in the mouse-imaging chamber and on the scanner bed. A 120-min PET acquisition was performed first with the Inveon-dedicated PET scanner, docked to the MM scanner. The average delay between the time of injection and start of the PET was 3.4 min.

Following the PET acquisition, each mouse received a 20-min high-resolution CT scan using the Inveon MM CT scanner. Throughout the scanning period, the animals were kept under 2 % isoflurane anesthesia. The PET list-mode data were dynamically sorted into 23 3D sinograms of span 3 and ring difference 79 (4×1, 3×2, 10×5, and 6×10 min) and, following Fourier rebinning, were reconstructed using a 2D ordered-subset expectation maximization algorithm (16 subsets, 4 iterations, and 2 EM iterations) into 128×128×159 image arrays with a 0.77-mm pixel size and a slice thickness of 0.796 mm. Random events were subtracted prior to reconstruction. Normalization of detector responses was also applied using a component-based method. All dynamic images were automatically corrected for radioactive decay due to manufacturer software settings. Quantitative calibration of PET images was performed by scanning 19.6 MBq of well-mixed ^{18}F solution inside a 56-ml plastic container. The CT scan was performed at two overlapping bed positions with detector–source rotating 360 ° around the animal with projections acquired every 0.5 ° (720 angles). CT images were reconstructed with a cone beam algorithm into 480×480×632 image arrays with a 206-μm pixel. Following the reconstruction, the CT images were spatially transformed to match the PET images. The CT scan served two purposes: to acquire an attenuation map for attenuation correction of PET images and for anatomical identification of mouse organs of interest in the study.

Image Analysis

Processing of reconstructed images was performed with PMOD software package (PMOD Technologies). 3D volumes of interest (VOIs) were drawn manually on the following “source” organs: the brain, lower large intestine (LLI), stomach, heart, kidneys, liver, lungs, pancreas, cortical bone, spleen, testes, thymus, gallbladder, uterus, and urinary bladder (Fig. 1). The organs were identified, and VOIs were drawn as irregular contours on the high-resolution CT images acquired for each mouse. The VOIs drawing was verified by a second operator.

The size of each VOI was smaller than the actual size of each organ in order to minimize the PET effects of spill in and spillover from adjacent organs. The VOIs, representing the cortical bone, were generated by first delineating the whole femur bone using the CT image and then setting a lower threshold of 50 % the maximum value of all voxels inside the initial

VOI and allowing for multiple contours. The liver VOI did not include the gallbladder, which was identified using the PET images. The VOIs were transferred to dynamic PET images, and the decay-corrected mean time-activity curves (TACs) were extracted for each target organ.

Dose Calculations

Following the extraction of time-activity curves, the residence times of radioactive [^{18}F]Mefway in each target organ and the absorbed doses in multiple source organs were computed using Matlab. Since in dose calculation, the actual activity over time is of interest, the decay correction was reversed prior to computation of residence times using the formula: $\mathrm{TAC}\,(t)=\mathrm{TAC}_{\mathrm{corr}}(t)x(\frac{\lambda}{\Delta t})x\frac{1-\exp(-\lambda\Delta t)}{\exp(\lambda t_s)}$. $\mathrm{TAC}_{\mathrm{corr}}$ is the decay-corrected TAC; λ is the decay constant for ^{18}F; Δt is the frame duration, and t_s is the start time of each frame.

The residence times R_i in the ith organ was computed using the formula:

$$R(i)=O_m(i)\times\int_0^\infty \mathrm{TAC}\,(i,t)\mathrm{dt}/A_{\mathrm{inj}} \quad (1)$$

where TAC (i,t) is the time activity curve for the ith organ (in becquerels per cubic centimeter); O_m (i) is the mass of the ith organ (in grams), and A_{inj} is the administered activity (in becquerels). The organ masses for the 30-g mouse model were taken from Table 1 in Keenan et al. [12] and divided by the average organ density of 1 g/cm^3 before being used in Eq. (1). Thus, the units for the residence times were (in becquerel-hour per becquerel administered).

The integral in Eq. (1) was computed using area under the curve (AUC) for each TAC. The integral between the time of [^{18}F] Mefway injection and start of the scan (2–3 min) was computed assuming linearity. The AUC between the start and the end of the scan was computed numerically from the acquired TAC using trapezoidal method. The integral between the end of the scan and infinity was computed analytically, assuming that the kinetics was governed by the radioactive decay of ^{18}F. The residence times for the remainder of the body were computed by subtracting the sum of all organs residence times from the maximum, physically allowed, whole-body residence time, which for ^{18}F is equal to 2.62 (=$T_{1/2}$/ln 2).

The dose absorbed by the ith target organ was computed as:

$$\mathrm{OD}(i)=\sum_j R(j)\times\mathrm{DF}(j,i) \quad (2)$$

where R (j) = residence time for the jth organ, DF (j,i) = dose factor between the jth source organ and the ith target organ. The dose factors, which are a function of mouse weight and relate the residence times in source organs to the absorbed dose in each target organ, were taken from Table 3 in Keenan et al. [12].

Further, the residence times for humans, R_h, were computed from mouse residence times, R_m, by using percent-kilogram per gram extrapolation, which assumes proportionality based on weight difference between species [14]:

$$R_h=R_m\times(O_h/B_h)/(O_m/B_m) \quad (3)$$

with O_h = human organ weight, O_m = mouse organ weight, B_h = human body weight, and B_m = mouse body weight.

The human body weight, B_h, and the human organ masses, O_h, were taken from OLINDA/EXM 1.1 for adult female and adult male phantoms, respectively. The mouse body weight, B_m, and the mouse organ masses were those of a 30-g mouse in the RADAR model [12]. The masses of the gallbladder and uterus that were used for estimation of human residence times were not included in the RADAR model, and instead, values measured directly by weighing the organs postmortem were used. The projected human doses were then computed for both male and female phantoms using OLINDA/EXM 1.1 software package with the human residence times, R_h, as input.

Post Scan Ex Vivo Procedures

Following *in vivo* imaging, the animals were sacrificed by decapitation while under anesthesia, and body organs were collected to determine postmortem residual activity and biodistribution. Whole organs and organ tissue samples were weighed and then counted individually for 60 s using a Capintec Caprac-R well counter. Radiation background was subtracted. Net count rates were divided by the weight of each tissue sample and decay corrected to the end of PET scan.

Results

The VOI delineation on CT images is illustrated in Fig. 1 that shows three coronal and one sagital views of a male mouse. In the early part of the scan, the kidneys present higher activity, while in the later part (90–120 min), the urinary bladder values are higher (Fig. 2). The specificity of [^{18}F]Mefway for 5-HT$_{1A}$ receptors is illustrated in Fig. 2c, which shows orthogonal PET slices through the brain of one of the subjects (average 0–30 min, bottom row) as well as an overlay with an MR template [15] (top row). Notice how the hippocampus, a brain region rich in 5-HT$_{1A}$ receptors, presents high tracer uptake. Representative TACs normalized to the injected activity in source organs are shown in Fig. 3. Table 1 lists the residence times of [^{18}F] Mefway in all the mouse organs. The largest values were found in the liver and bone followed closely by urinary bladder and kidneys. The largest absorbed dose was received by the urinary bladder (“critical organ”) in both female (3.26E+02±3.01E+01 mSv/MBq) and male (3.21E+02±1.51E+01 mSv/MBq) mice (Table 2). The mean residence times for both adult female and male phantoms are listed in Table 3, and the mean projected human doses are listed in Table 4. The urinary bladder received the highest absorbed dose for both female and male phantoms. The mean effective doses were 1.21E–02±3.79E–04 mSv/MBq (adult female phantom) and 1.13E–02± 4.93E–04 mSv/MBq (adult male phantom).

Table 5 lists side by side, in descending order, the normalized *ex vivo* count rates and the *in vivo* activity at the end of the scans (last 10-min frame). The largest *ex vivo* count rates were found in the gallbladder, bone (skull), urinary bladder, kidney, stomach, and liver. The largest *in vivo* activity values were found in the urinary bladder, gallbladder, kidneys, uterus, stomach, bone (femur), and liver. The correlation between *ex vivo* and *in vivo* values was low (r=0.34, p=0.0009; Fig. 4a). However, by just removing the urinary bladder from consideration, the correlation increased considerably (r=0.83, p=0.0001; Fig. 4b).

Discussion

Biodistribution and dosimetry studies are conducted before a PET radiotracer is used in humans in order to estimate the internal radiation dose absorbed by each human organ. This allows an assessment of radiation safety of the radiotracer and the number of studies that can be safely conducted annually. The availability of preclinical PET and CT scanners and the development of physical models for internal dose assessment in small animals allow preliminary evaluation of tracer biodistribution in mice or rats and provide initial estimates

of human doses. In this study, the absorbed radiation doses in mouse organs of [^{18}F]Mefway radiotracer were evaluated using whole-body PET/CT and a mouse model of dose assessment.

Elimination of [^{18}F]Mefway from mouse body occurred via urinary system as indicated by the kidney activity preceding the urinary bladder as well as by the much higher activity in the urinary tract than in the digestive system (e.g., stomach and LLI). The urinary bladder was the critical organ with the largest absorbed dose. High absorbed doses were also registered in the kidneys, liver, and osteogenic cells.

We compared *ex vivo* count rates from organ tissue samples measured postscan with the *in vivo* activity values at the end of the PET scan. The poor correlation found initially could be attributed to radioactivity measured in hollow organs, such as the urinary bladder and intestines, as PET values were a measure of organ content, while *ex vivo* count rates were a measure of radioactivity in the organ walls. By removing the urinary bladder from consideration, the correlation improved significantly (Fig. 4b). We also found that the gallbladder ranked higher in the *ex vivo* data than in the *in vivo*, which could be explained by the partial volume effects in PET caused by the very small size of this organ. The spillover activity from the urinary bladder caused activity in the uterus, which is a neighboring organ to rank higher in the *in vivo* data than in the *ex vivo*.

Translation of residence time in the mouse bone to humans presents a few challenges. First, the fast metabolism of the mouse compared to human may cause a rapid presence of radioactive fluorine-18 in the blood and a higher accumulation in the mouse bone, as indicated by the high residence time. However, the monkey PET studies conducted so far showed no significant uptake of [^{18}F]Mefway in the skull and, therefore, low defluorination [9]. Assuming the human's breaking down of [^{18}F]Mefway is rather similar to the monkey's than it is expected that the human doses in the bone as projected by this study be overestimated. Second, in the mouse model, the whole skeleton is modeled, while in human, the bone surfaces (cortical bone) are separated from red marrow. It is also difficult to separate the bone activity from that of red marrow in the mouse due to limited resolution of PET. To estimate the impact of large changes in the total number of disintegration in the bone on the absorbed dose in the bone itself and other organs, we performed a simulation exercise in which the bone residence time was increased or decreased by a factor of 10. This perturbation induced changes of about 25 % on average in absorbed dose in osteogenic cells and about 5 % in red marrow, but less than 1.5 % in the other organs and in the effective dose for both female and male phantoms.

Currently, the RADAR model does not provide dose factors and masses for all the organs that are relevant to human dosimetry, such as the gallbladder and uterus. For the purpose of estimating the mouse doses, the residence times for these two organs were lumped with the rest of the body. However, when we extrapolated the residence times from mouse to human, both organs were included in calculation with their masses measured experimentally in the postmortem analysis.

Because of the chemical similarity between [^{18}F]Mefway and [^{11}C]WAY, we used previous dosimetry studies with [^{11}C]WAY 100,635 [16] as a basis for comparison. The projected [^{18}F]Mefway dose values for human organs ranked similarly and correlated well (r=0.82, p<0.01) to those of [^{11}C]WAY 100,635 in humans, with the urinary bladder and kidney receiving the highest dose in both cases. Note that in the mouse model of [^{18}F]Mefway, the urinary bladder was the critical organ as was the case with [^{11}C]WAY 100,635 in humans. Preclinical findings with [^{11}C]WAY 100,635 in rats had predicted that the liver was the critical organ [16]. Despite kinetic similarities, direct comparisons between the two tracers

cannot be easily performed as one is labeled with ^{18}F and the other with ^{11}C. The two isotopes deposit a different amount of energy in the tissue due to different disintegration constants and positron kinetic energies.

One of the goals of a human dosimetry study is to estimate the maximum activity that can be received by a human subject annually without surpassing the dose limits allowed. According to the federal regulations specified in Title 21 CFR 361.1, the annual limit [17], the radiation doses to the whole body, gonads, active blood-forming organs, and lens of the eye should not exceed 50 mSv (5 rem) annually and 30 mSv (3 rem) for a single study. The dose absorbed by all other organs should not exceed 150 mSv (15 rem) annually and 50 mSv (5 rem). The urinary bladder is the limiting (or critical) organ for [^{18}F]Mefway according to the present study and therefore dictates which the maximum injected activity per study is. Based on our projected human doses for the urinary bladder, the limits for injected [^{18}F]Mefway activity would be 1,458 MBq (39 mCi) for the adult female model and 1,563 MBq (42 mCi) for the male model. At 185 MBq (5 mCi) administered per study these limits should allow multiple studies per year for each subject. Our estimated limit for administered activity in a single human study appears to be higher than expected. In comparison, according to International Commission on Radiological Protection Publication 106, the adult-limiting dose for 2-deoxy-2-[^{18}F]fluoro-D-glucose ([^{18}F] FDG) in adults is 0.13 mSv/MBq which translates into 384 MBq (10 mCi) per study. One possible explanation for this finding is that urinary bladder dosimetry (and possibly the kidneys) is lower in mouse than in humans. [^{11}C]WAY 100,635 dosimetry studies have found that the urinary bladder and kidney dosimetry were higher in human than in rat (cited in Parsey et al. [16]). Since no human dosimetry studies have been performed yet in humans, we are unable to evaluate at this time if this is the case for [^{18}F]Mefway or the extent of differences between the two species. In conducting human dosimetry studies, there are existing strategies aimed to lower the absorbed dose in critical organs. For example, as studies with [^{18}F]FDG in humans have shown that the limiting dose in the urinary bladder wall can be reduced by asking the subject to hydrate before the scan and voiding the bladder postscan [18].

Although not meant to be a substitute for a complete dose assessment in humans, the current study is a useful preliminary data set as [^{18}F]Mefway is being translated to humans. As a future research, we are planning [^{18}F]Mefway dosimetry studies in human subjects that will assist to verify and validate the accuracy of the animal model results presented in this study.

Acknowledgments

The project described was supported by a grant, number NIH R21 AG030524, from the National Institute of Aging (NIA), which was awarded to Jogeshwar Mukherjee. The authors would also like to thank Ritu Kant and Sarah P Nguyen for their help in validation of regions of interest on mouse organs.

References

1. Kumar JS, Mann JJ. PET tracers for 5-HT(1A) receptors and uses thereof. Drug Discov Today. 2007; 12:748–756. [PubMed: 17826688]
2. Paterson LM, Kornum BR, Nutt DJ, Pike VW, Knudsen GM. 5-HT radioligands for human brain imaging with PET and SPECT. Med Res Rev. 201110.1002/med.20245
3. Savitz J, Lucki I, Drevets WC. 5-HT(1A) receptor function in major depressive disorder. Prog Neurobiol. 2009; 88:17–31. [PubMed: 19428959]
4. Akimova E, Lanzenberger R, Kasper S. The serotonin-1A receptor in anxiety disorders. Biol Psychiatry. 2009; 66:627–635. [PubMed: 19423077]
5. Assem-Hilger E, Lanzenberger R, Savli M, et al. Central serotonin 1A receptor binding in temporal lobe epilepsy: a [carbonyl-(11)C]WAY-100635 PET study. Epilepsy Behav. 2010; 19:467–473. [PubMed: 20850389]

6. Parsey RV. Serotonin receptor imaging: clinically useful? J Nucl Med. 2010; 51:1495–1498. [PubMed: 20847181]
7. Bert B, Fink H, Rothe J, Walstab J, Bonisch H. Learning and memory in 5-HT(1A)-receptor mutant mice. Behav Brain Res. 2008; 195:78–85. [PubMed: 18396339]
8. King MV, Marsden CA, Fone KC. A role for the 5-HT(1A), 5-HT(4) and 5-HT(6) receptors in learning and memory. Trends Pharmacol Sci. 2008; 29(9):482–492. [PubMed: 19086256]
9. Saigal N, Pichika R, Easwaramoorthy B, et al. Synthesis and biologic evaluation of a novel serotonin 5-HT1A receptor radioligand, 18F-labeled mefway, in rodents and imaging by PET in a nonhuman primate. J Nucl Med. 2006; 47:1697–1706. [PubMed: 17015907]
10. Fong V, Faheem S, Sevrioukov E, et al. ^{18}F-Mefway microPET imaging in rat brains [abstract]. J Nucl Med. 2011; 52(Suppl 1):1571.
11. Wooten DW, Moraino JD, Hillmer AT, et al. *In vivo* kinetics of [F-18]MEFWAY: a comparison with [C-11]WAY100635 and [F-18] MPPF in the nonhuman primate. Synapse. 2011; 65:592–600. [PubMed: 21484878]
12. Keenan MA, Stabin MG, Segars WP, Fernald MJ. RADAR realistic animal model series for dose assessment. J Nucl Med. 2010; 51:471–476. [PubMed: 20197451]
13. Stabin MG, Sharkey RM, Siegel JA. RADAR commentary: evolution and current status of dosimetry in nuclear medicine. J Nucl Med. 2011; 52:1156–1161. [PubMed: 21680699]
14. Kirschner AS, Ice RD, Beierwaltes WH. Radiation-dosimetry of I-131-19-iodocholesterol: the pitfalls of using tissue concentration data —reply. J Nucl Med. 1975; 16:248–249.
15. Ma Y, Smith D, Hof PR, Foerster B, et al. *In vivo* 3D digital atlas database of the adult C57BL/6 J mouse brain by magnetic resonance microscopy. Front Neuroanat. 2008; 2:1–10. [PubMed: 18958199]
16. Parsey RV, Belanger MJ, Sullivan GM, et al. Biodistribution and radiation dosimetry of 11C-WAY100,635 in humans. J Nucl Med. 2005; 46:614–619. [PubMed: 15809484]
17. Food and Drug Administration. Title 21 CFR 361.1 radioactive drugs for certain research uses. National Archives and Records Administration, Office of the Federal Register; Washington DC: 2011. p. 325-330.
18. Dowd MT, Chen CT, Wendel MJ, Faulhaber PJ, Cooper MD. Radiation dose to the bladder wall from 2-[18F]fluoro-2-deoxy-D-glucose in adult humans. J Nucl Med. 1991; 32:707–712. [PubMed: 2013811]

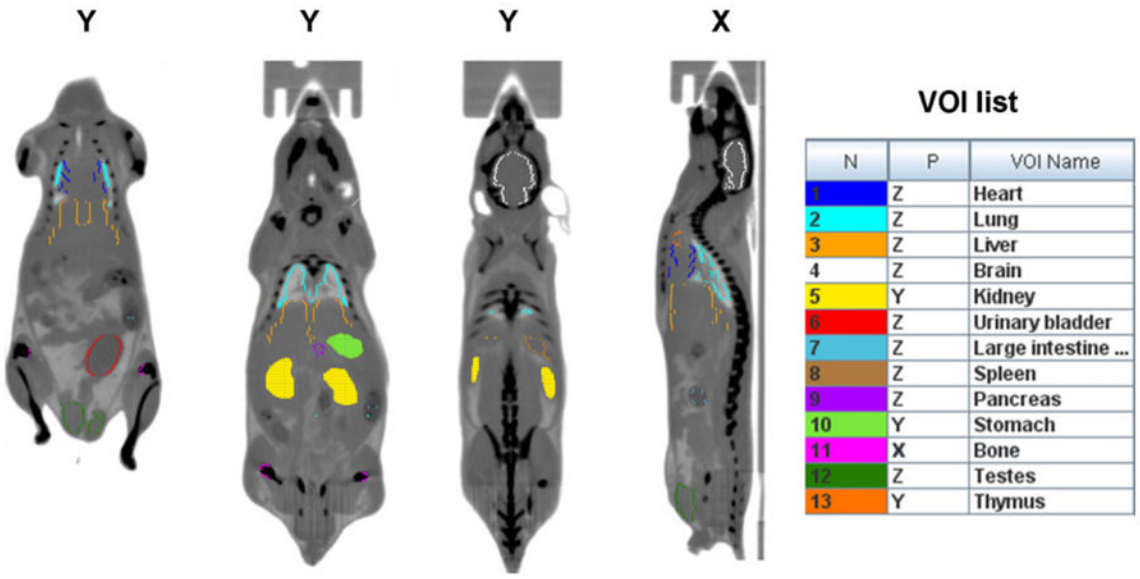

Fig. 1.

Representative mouse CT images in coronal (*Y*) and sagital (*X*) views showing the drawing of volume of interest (*VOIs*) on different organs. The CT images were acquired at two overlapping bed positions. The VOIs drawn in the same view as the one shown appear as filled contours, while the ones drawn in different view appear as colored contours. The complete list of VOIs is shown on the *right handside*.

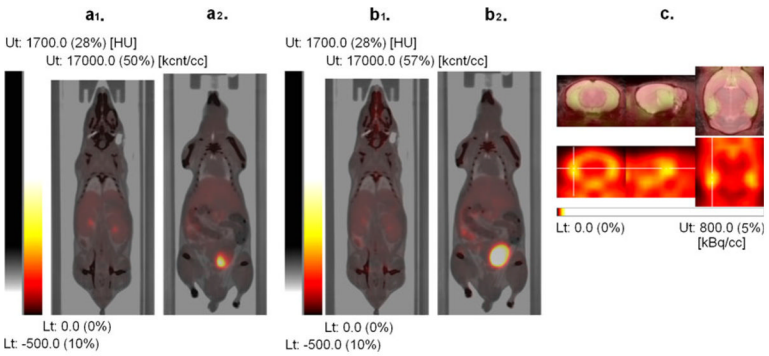

Fig. 2.

Fused PET-CT images with PET images from the first 30 min (**a** *1*, **a** *2*) and from 90 to 120 min (**b** *1*, **b** *2*) after injection of [^{18}F] Mefway (weighted summation of dynamic frames). The early image (**a** *1*) shows higher tracer uptake in the kidney compared with the late images (**b** *1*), while the late image (**b** *2*) shows higher tracer uptake in the urinary bladder than the early image (**a** *2*). This illustrates that the elimination of the tracer from mouse body occurs primarily via urinary system. (**c**) PET images of the mouse brain (*bottom panel*) showing high selective binding of [^{18}F]Mefway in the hippocampus (marked with orthogonal crosshairs), a region rich in 5-HT$_{1A}$ receptors. Images were coregistered to an MR mouse brain template (*top panel*, *fused image*) [17].

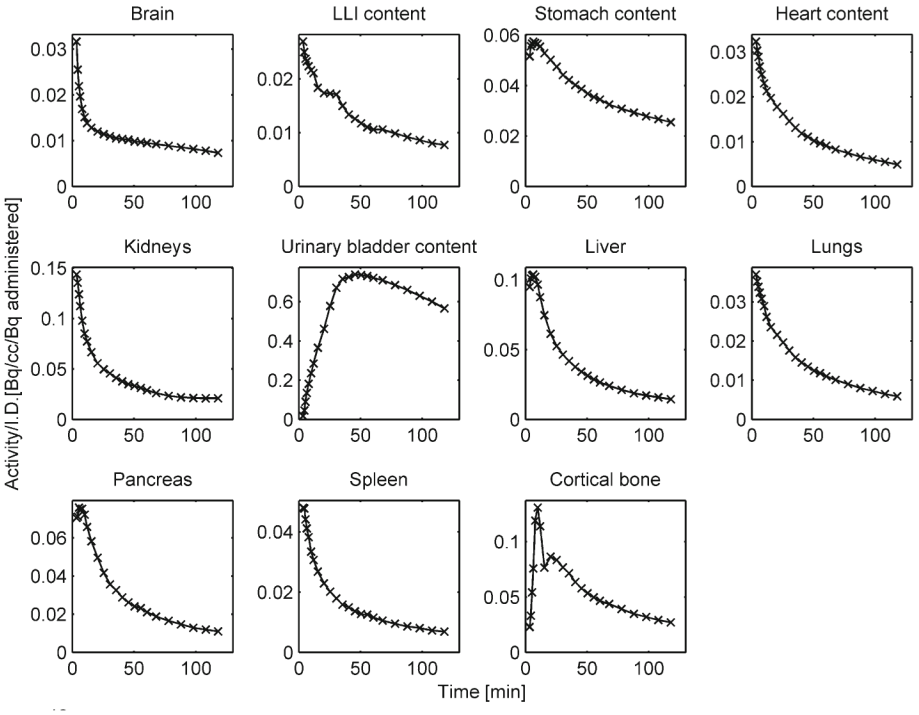

Fig. 3.

Representative [^{18}F]Mefway time-activity curves (not decay corrected) normalized to the injected activity from multiple mouse (male) organs: the brain, lower large intestine (*LLI*), stomach, heart, kidneys, urinary bladder, liver, lungs, pancreas, spleen, and cortical bone are shown.

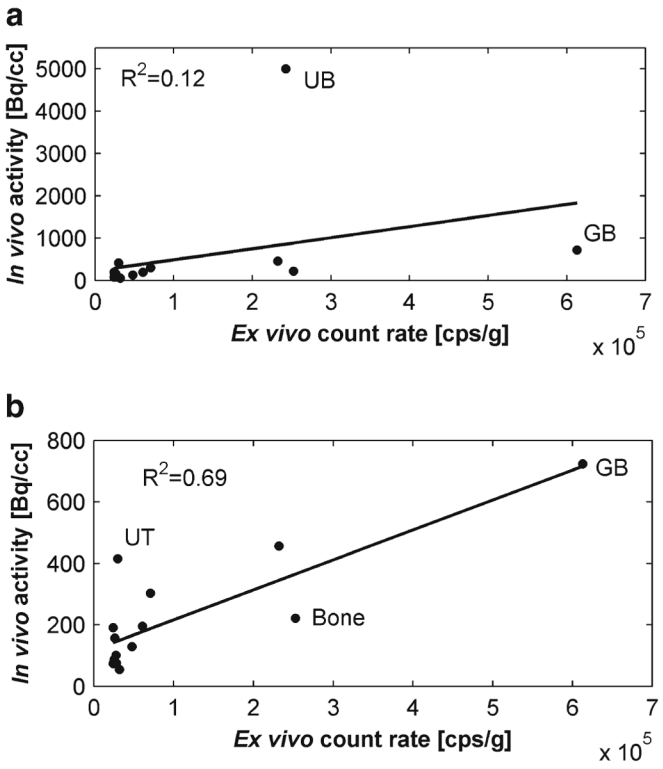

Fig. 4.

Scatter plots of the *in vivo* activity (mean of male and female mice) as measured with PET over last 10 min of the scan estimated using whole organ VOIs versus mean *ex vivo* count rate from organ tissue samples normalized to the sample weight. Selective points corresponding to the urinary bladder (*UB*), gallbladder (*GB*), uterus (*UT*), and bone are labeled. **a** Subplot shows data from all the organs, together with the linear regression line. **b** Subplot shows the same data as in (**a**) except for the urinary bladder along with a new regression line.

Table 1

Residence times (in becquerel-hour per becquerel administered) of [^{18}F]Mefway in mouse organs

Source organs	Female 1	Female 2	Female 3	Female average (±SD)	Male 1	Male 2	Male 3	Male average (±SD)
Brain	2.93E–02	3.88E–02	3.58E–02	3.46E–02±4.86E–03	3.67E–02	3.18E–02	2.26E–02	3.04E–02±7.16E–03
LLI content	2.60E–02	6.99E–02	8.20E–02	5.93E–02±2.95E–02	5.58E–02	5.51E–02	3.20E–02	4.76E–02±1.35E–02
Stomach content	1.17E–02	9.29E–03	1.38E–02	1.16E–02±2.26E–03	1.16E–02	1.35E–02	9.62E–03	1.16E–02±1.94E–03
Heart content	1.75E–02	1.75E–02	1.93E–02	1.81E–02±1.04E–03	1.23E–02	1.51E–02	1.02E–02	1.25E–02±2.46E–03
Kidneys	8.77E–02	5.85E–02	1.12E–01	8.61E–02±2.68E–02	1.07E–01	1.40E–01	4.90E–02	9.87E–02±4.61E–02
Liver	4.00E–01	2.78E–01	3.76E–01	3.51E–01±6.46E–02	2.79E–01	3.40E–01	2.36E–01	2.85E–01±5.23E–02
Lungs	6.53E–03	4.90E–03	7.45E–03	6.29E–03±1.29E–03	4.54E–03	5.03E–03	4.50E–03	4.69E–03±2.95E–04
Pancreas	5.00E–02	4.39E–02	7.39E–02	5.59E–02±1.59E–02	3.71E–02	6.57E–02	3.18E–02	4.49E–02±1.82E–02
Cortical bone	2.69E–01	2.22E–01	3.95E–01	2.95E–01±8.95E–02	1.88E–01	2.37E–01	4.57E–01	2.94E–01±1.43E–01
Spleen	1.40E–02	9.28E–03	1.63E–02	1.32E–02±3.58E–03	1.03E–02	2.20E–02	6.46E–03	1.29E–02±8.09E–03
Testes	N/A	N/A	N/A	N/A	5.65E–03	1.14E–02	3.60E–03	6.88E–03±4.04E–03
Thymus	9.06E–04	1.01E–03	1.19E–03	1.04E–03±1.44E–04	8.17E–04	8.74E–04	6.82E–04	7.91E–04±9.86E–05
Urinary bladder content	1.95E–01	2.08E–01	1.73E–01	1.92E–01±1.77E–02	1.81E–01	1.86E–01	1.99E–01	1.89E–01±9.29E–03
Total body	1.53E+00	1.68E+00	1.33E+00	1.51E+00±1.76E–01	1.71E+00	1.52E+00	1.58E+00	1.60E+00±9.71E–02

SD standard deviation, *N/A* not available

Mol Imaging Biol. Author manuscript; available in PMC 2013 October 28.

Table 2

Absorbed mouse organ doses (in millisieverts per megabecquerel) for [^{18}F]Mefway

Organs	Female 1	Female 2	Female 3	Female average (±SD)	Male 1	Male 2	Male 3	Male average (±SD)
Brain	1.62E+01	1.91E+01	1.71E+01	1.74E+01±1.51E+00	1.87E+01	1.66E+01	1.53E+01	1.69E+01±1.68E+00
LLI wall	1.44E+01	2.29E+01	2.35E+01	2.03E+01±5.09E+00	2.07E+01	1.98E+01	1.56E+01	1.87E+01±2.70E+00
Small intestine	9.85E+00	1.07E+01	9.06E+00	9.86E+00±7.97E–01	1.08E+01	9.97E+00	9.90E+00	1.02E+01±4.97E–01
Stomach wall	2.70E+01	2.39E+01	2.88E+01	2.66E+01±2.52E+00	2.67E+01	2.91E+01	2.32E+01	2.63E+01±2.95E+00
Heart wall	1.88E+01	1.91E+01	1.88E+01	1.89E+01±1.63E–01	1.68E+01	1.74E+01	1.55E+01	1.66E+01±9.48E–01
Kidneys	4.06E+01	3.12E+01	4.84E+01	4.01E+01±8.62E+00	4.81E+01	5.90E+01	2.71E+01	4.47E+01±1.62E+01
Liver	3.58E+01	2.85E+01	3.34E+01	3.26E+01±3.71E+00	2.87E+01	3.19E+01	2.54E+01	2.87E+01±3.26E+00
Lungs	1.97E+01	1.79E+01	2.06E+01	1.94E+01±1.36E+00	1.73E+01	1.77E+01	1.91E+01	1.80E+01±9.47E–01
Pancreas	2.79E+01	2.61E+01	3.51E+01	2.97E+01±4.76E+00	2.44E+01	3.35E+01	2.12E+01	2.64E+01±6.35E+00
Osteogenic cells	2.11E+01	1.97E+01	2.56E+01	2.21E+01±3.10E+00	1.83E+01	1.95E+01	2.94E+01	2.24E+01±6.06E+00
Spleen	2.31E+01	1.93E+01	2.47E+01	2.23E+01±2.78E+00	2.05E+01	3.08E+01	1.59E+01	2.24E+01±7.64E+00
Testes	N/A	N/A	N/A	N/A	1.39E+01	1.67E+01	1.20E+01	1.42E+01±2.35E+00
Thyroid	1.57E+01	1.71E+01	1.69E+01	1.66E+01±7.62E–01	1.58E+01	1.53E+01	1.48E+01	1.53E+01±5.32E–01
Urinary bladder wall	3.31E+02	3.53E+02	2.94E+02	3.26E+02±3.01E+01	3.09E+02	3.16E+02	3.38E+02	3.21E+02±1.51E+01
Total body	7.33E+00	6.65E+00	8.23E+00	7.40E+00±7.93E–01	6.51E+00	7.41E+00	7.08E+00	7.00E+00±4.56E–01

SD standard deviation, *N/A* not available

Table 3

Human residence times (in becquerel–hour per becquerel administered) estimates of [^{18}F]Mefway based on mouse residence times and modeled organ mass differences between the two species

Source organs	Female average (±SD)	Male average (±SD)
Brain	3.21E–02±4.47E–03	3.09E–02±7.29E–03
LLI content	5.88E–03±2.92E–03	4.57E–03±1.30E–03
Stomach content	1.03E–02±2.02E–03	1.08E–02±1.83E–03
Heart content	6.56E–03±3.76E–04	5.53E–03±1.08E–03
Kidneys	2.78E–02±8.62E–03	3.21E–02±1.49E–02
Liver	1.01E–01±1.84E–02	1.03E–01±1.90E–02
Lungs	2.07E–02±4.23E–03	1.79E–02±1.12E–03
Pancreas	5.52E–03±1.57E–03	4.56E–03±1.85E–03
Cortical bone	6.46E–02±1.96E–02	5.14E–02±2.50E–02
Spleen	6.39E–03±1.73E–03	7.07E–03±4.43E–03
Testes	N/A	5.57E–04±3.28E–04
Thymus	5.69E–04±7.76E–05	4.21E–04±5.26E–05
Urinary bladder content	4.04E–02±3.73E–03	4.87E–02±2.43E–03
Gall bladder	1.57E–03±6.05E–04	1.71E–03±5.48E–04
Uterus	9.62E–03±3.55E–03	N/A
Total body	1.26E+00±1.45E–01	1.61E+00±1.00E–01

SD standard deviation, *N/A* not available

Table 4

Human doses (in millisieverts per megabecquerel) estimates for [^{18}F]Mefway generated with OLINDA/EXM 1.1 software using residence times estimated from the mouse residence times

Target organs	Female average (±SD)	Male average (±SD)
Adrenals	1.10E–02±4.04E–04	1.05E–02±5.78E–04
Brain	8.03E–03±9.04E–04	6.86E–03±1.18E–03
Breasts	7.02E–03±6.29E–04	6.88E–03±3.61E–04
Gallbladder wall	1.36E–02±1.12E–03	1.37E–02±1.26E–03
LLI wall	1.38E–02±1.83E–03	1.27E–02±9.54E–04
Small intestine	9.88E–03±7.92E–04	1.06E–02±5.51E–04
Stomach wall	1.36E–02±2.31E–04	1.31E–02±8.96E–04
ULI wall	1.05E–02±8.57E–04	1.04E–02±5.20E–04
Heart wall	1.07E–02±5.13E–04	9.97E–03±4.46E–04
Kidneys	2.37E–02±5.47E–03	2.49E–02±9.25E–03
Liver	2.01E–02±2.84E–03	1.64E–02±2.40E–03
Lungs	9.32E–03±6.96E–04	7.65E–03±2.38E–04
Muscle	8.35E–03±7.19E–04	8.36E–03±4.22E–04
Ovaries	1.10E–02±9.29E–04	N/A
Pancreas	1.83E–02±3.03E–03	1.53E–02±3.64E–03
Red marrow	8.07E–03±5.21E–04	7.95E–03±3.45E–04
Osteogenic cells	1.74E–02±3.00E–04	1.50E–02±1.27E–03
Skin	6.44E–03±6.07E–04	6.49E–03±3.52E–04
Spleen	1.34E–02±2.01E–03	1.26E–02±4.70E–03
Testes	N/A	7.13E–03±1.23E–03
Thymus	9.59E–03±4.45E–04	8.07E–03±4.78E–04
Thyroid	7.81E–03±7.86E–04	8.43E–03±5.00E–04
Urinary bladder wall	3.43E–02±3.14E–03	3.20E–02±1.00E–03
Uterus	2.80E–02±7.62E–03	N/A
Total body	9.15E–03±5.42E–04	8.87E–03±3.75E–04
Effective dose equivalent	1.41E–02±6.24E–04	1.25E–02±9.71E–04
Effective dose	1.21E–02±3.79E–04	1.13E–02±4.93E–04

SD standard deviation, *N/A* not available

Table 5

Comparison between the *ex vivo* counting rates of organ tissue samples and *in vivo* activity as measured with PET (last 10 min of scan time)

Organs	*Ex vivo* counting rate (±SEM) (kBq/cm^3)	Organs	*In vivo* activity (±SEM) (kBq/cm^3)
Gallbladder	6.1E+05±1.1E+05	Urinary bladder content	5.0E+03±6.8E+02
Bone (skull)	2.5E+05±2.5E+04	Gallbladder content	7.2E+02±1.1E+02
Urinary bladder wall	2.4E+05±1.0E+05	Kidneys	4.6E+02±8.8E+01
Kidney	2.3E+05±3.0E+04	Uterus	4.2E+02±5.6E+01
Stomach wall	7.1E+04±9.6E+03	Stomach content	3.0E+02±3.3E+01
Liver	6.1E+04±2.7E+03	Cortical bone	2.2E+02±4.1E+01
LLI wall	4.8E+04±1.6E+04	Liver	2.0E+02±1.3E+01
Testes	3.2E+04±1.6E+04	Pancreas	1.9E+02±2.9E+01
Uterus	3.0E+04±7.6E+03	Spleen	1.6E+02±3.3E+01
Heart	2.8E+04±3.1E+03	LLI content	1.3E+02±1.9E+01
Brain	2.8E+04±3.5E+03	Brain	1.0E+02±8.1E+00
Spleen	2.6E+04±2.7E+03	Thymus	8.7E+01±5.8E+00
Thymus	2.5E+04±2.6E+03	Heart	7.7E+01±3.6E+00
Lungs	2.5E+04±1.2E+03	Lungs	7.7E+01±5.3E+00
Pancreas	2.4E+04±2.3E+03	Muscle	7.4E+01±5.8E+00
Muscle	2.4E+04±2.4E+03	Testes	5.5E+01±1.1E+01

SEM standard error of the mean